catalysts

MDPI

Article

Highly Loaded and Dispersed Ni_2P/Al_2O_3 Catalyst with High Selectivity for Hydrogenation of Acetophenone

Junen Wang *, Yanling Wang, Gaoli Chen and Zhanjun He

Key Laboratory of Energetic Materials, College of Chemistry and Materials Science, Huaibei Normal University, Huaibei 235000, China; wangyl2002@163.com (Y.W.); gaolichen@chnu.edu.cn (G.C.); hzj003@163.com (Z.H.)

* Correspondence: junenwang@chnu.edu.cn; Tel./Fax: +86-561-3803233

Received: 8 July 2018; Accepted: 27 July 2018; Published: 30 July 2018

Abstract: Highly loaded and dispersed Ni_2P/Al_2O_3 catalyst was prepared by the phosphidation of Ni/Al_2O_3 catalyst with Ni loading of 80 wt.% in liquid phase and compared with the Ni/Al_2O_3 catalyst for the hydrogenation of acetophenone. X-ray diffraction (XRD), transmission electron microscopy (TEM) and X-ray photoelectron spectroscopy (XPS) etc. were used to characterize the textural and structural properties of the prepared catalysts. It was found that the Ni/Al_2O_3 and Ni_2P/Al_2O_3 catalyst possessed high surface area, loading and dispersion. The Ni/Al_2O_3 catalyst had higher apparent activity while the Ni_2P/Al_2O_3 catalyst had higher intrinsic activity for the hydrogenation of acetophenone (AP). Remarkably, the Ni_2P/Al_2O_3 catalyst exhibited high selectivity to 1-phenylethanol, due to repulsion of the phosphorous ($P^{\delta-}$) for phenyl group and attraction of the nickel ($Ni^{\delta+}$) for oxygen atom of carbonyl group, leading to preferential hydrogenation of carbonyl group in acetophenone. The effect of the particle size of the catalyst on the chemical selectivity might be another reason for high selectivity on the Ni_2P/Al_2O_3 catalyst.

Keywords: supported Ni_2P catalyst; supported Ni catalyst; hydrogenation; acetophenone; 1-phenylethanol

1. Introduction

1-phenylethanol (PHE), is a significant chemical intermediate and frequently used in the food, pharmaceutical, cosmetic and polymer industries [1], which can be obtained by the selective hydrogenation of acetophenone (AP) on supported metal catalysts. The hydrogenation of AP is usually performed on noble metal catalysts such as Ru [2,3], Pd [4,5], Pt [6,7], and so on. The hydrogenation of AP on Pt and Ru catalysts exhibits high selectivity for the hydrogenation of aromatic ring and poor selectivity for PHE [3,6]. Though supported Ru catalysts had high selectivity for the hydrogenation of carbonyl group of AP to form PHE, it is also active for consecutively converting PHE to ethylbenzene (EB), due to hydrogenolysis [5]. The non-noble metal catalysts, such as Cu [8,9], Co [10,11] and Ni [12–14], are also investigated for the hydrogenation of AP. Among them, the Ni-based catalysts are the most widely used for the hydrogenation of AP. The main product on the Ni-based catalysts is PHE, but variable quantities of byproducts such as cyclohexylmethylketone (CHMK), 1-cyclohexylethanol (CHE) and EB are found with increase of reaction temperature [13,14].

Very recently, Costa and his co-authors found that the hydrogenation of AP on the SiO_2 supported $Ni_2P/Ni_{12}P_5$ catalysts exhibited high selectivity to PHE [15]. Unfortunately, single-phase Ni_2P or $Ni_{12}P_5$ catalyst was not investigated for the hydrogenation of AP. In addition, the supported $Ni_2P/Ni_{12}P_5$ catalysts were prepared by wetness impregnation method using the nickel organometallic salts as precursor. This method is difficult for preparing the catalyst containing metal content

higher than 50 wt.%, due to the solubility of the precursor. Using thermal decomposition of nickel organometallic salts to prepare metal phosphides, the coordination agents remain in the catalysts and must be washed by the large amount of solvent, resulting in the burdens of post-treatment.

Previously, we have successfully prepared supported Ni_2P catalysts with high loading and dispersion by liquid phase phosphidation of supported Ni catalysts [16,17]. In this work, the Ni_2P/Al_2O_3 catalyst was prepared using the same method by phosphidation of Ni/Al_2O_3 catalyst. The hydrogenation of AP on the Ni_2P/Al_2O_3 and Ni/Al_2O_3 catalyst was investigated and it was found that the Ni_2P/Al_2O_3 catalyst exhibited higher intrinsic activity and selectivity to PHE than the Ni/Al_2O_3 catalyst.

2. Results and Discussion

2.1. Textural and Structural Properties of the Fresh Catalysts

X-ray diffraction (XRD) patterns of the Ni/Al_2O_3 and Ni_2P/Al_2O_3 catalyst are shown in Figure 1. For the pattern of Ni/Al_2O_3 catalyst, the peaks at 44.5°, 51.9° and 76.4° were indexed to (111), (200) and (220) planes of metallic nickel (PDF#65-0380), respectively. The average crystallite size of metallic Ni in the Ni/Al_2O_3 catalyst was estimated to be about 4.2 nm (Table 1), according to the Scherrer equation and the full width at half maximum (FWHM) of the (111) diffraction peak at 44.5°. No distinct reflection peaks of Al_2O_3 were found. For the pattern of Ni_2P/Al_2O_3 catalyst, the peaks around 40.7°, 44.6°, 47.4°and 54.2° were indexed to (111), (201), (210) and (300) planes of Ni_2P (PDF#65-1989), respectively. The average crystallite size of Ni_2P was estimated to be about 6.8 nm (Table 1) by the Scherrer equation and the (111) diffraction peak at 40.7°.

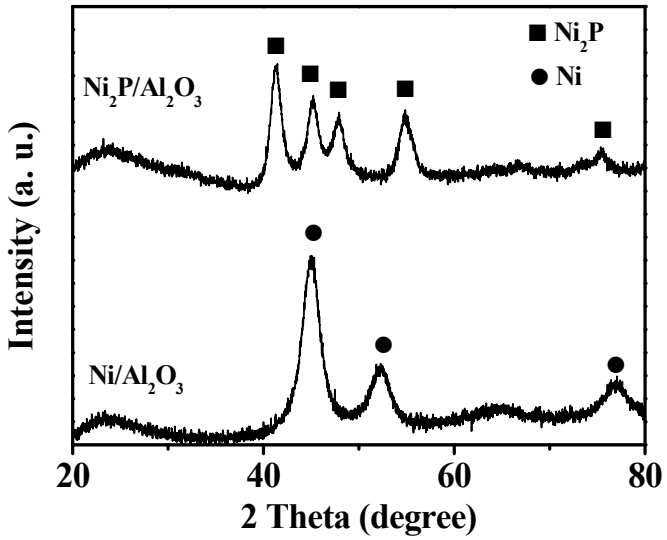

Figure 1. X-ray diffraction (XRD) patterns of the Ni/Al_2O_3 and Ni_2P/Al_2O_3 catalyst.

Table 1. Textural and structural properties of the Ni/Al_2O_3 and Ni_2P/Al_2O_3 catalyst.

Catalyst	S_{BET} (m^2/g)	Pore Volume (cm^3/g)	Pore Size (nm)	D (nm)	
				XRD	TEM
Ni/Al_2O_3	258	1.69	20.5	4.2	5.8
Ni_2P/Al_2O_3	145	0.70	15.6	6.8	8.2

Figure 2 shows the transmission electron microscope (TEM) images of Ni/Al_2O_3 and Ni_2P/Al_2O_3 catalyst. The two catalysts showed fairly uniform nanoparticles, indicating that metallic Ni and Ni_2P particles on the Al_2O_3 support were highly dispersed, although the loading of Ni was high to 80 wt.%

in the Ni/Al_2O_3 catalyst. The average particle sizes of Ni and Ni_2P in the two catalysts were 5.8 and 8.2 nm (Table 1), respectively, lager than those calculated by the Scherrer equation, probably due to the presence of other nickel species.

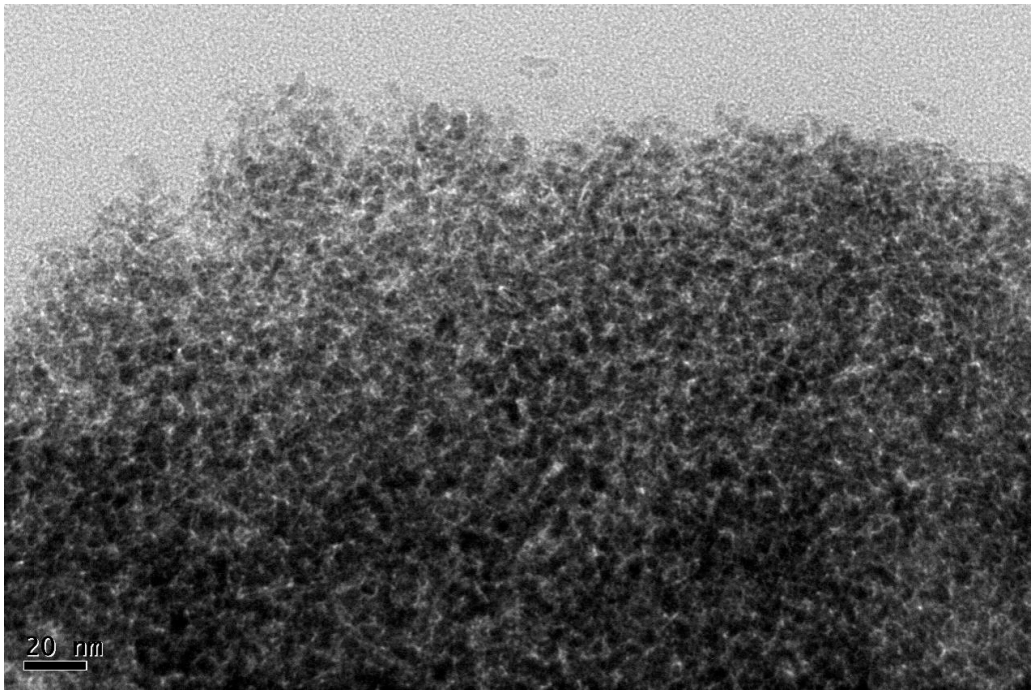

(**a**)

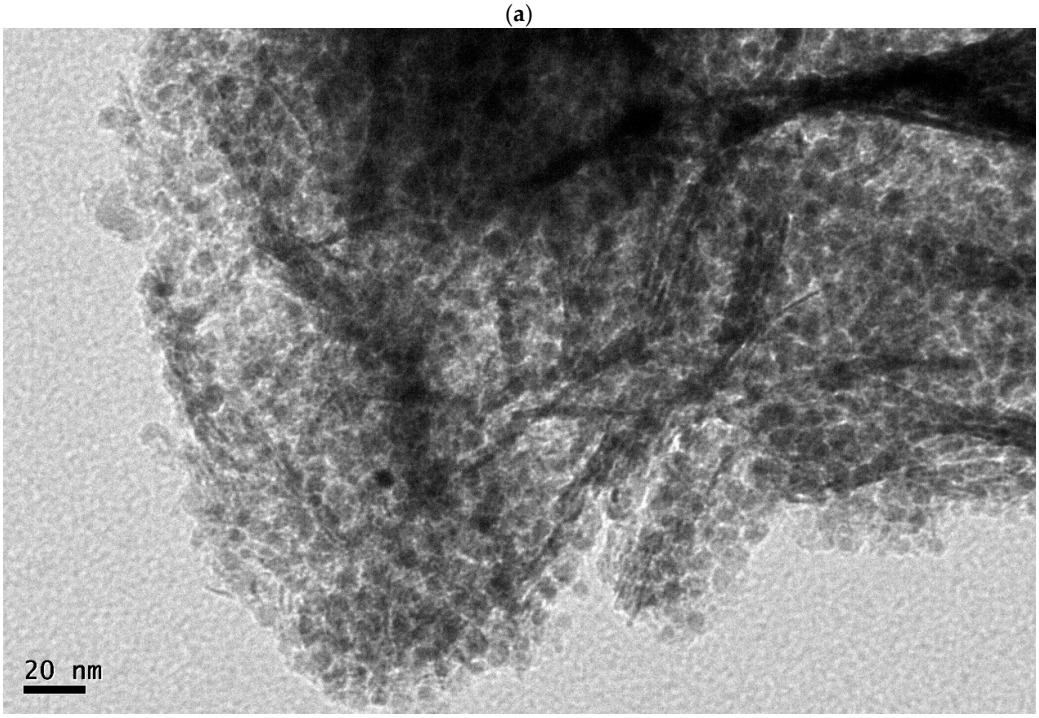

(**b**)

Figure 2. Transmission electron microscope (TEM) images of the Ni/Al_2O_3 (**a**) and Ni_2P/Al_2O_3 (**b**) catalyst.

Table 1 also gives the information of the Brunauer-Emmett-Teller (BET) surface areas, pore volumes and pore sizes for the Ni/Al_2O_3 and Ni_2P/Al_2O_3 catalyst. The surface area, pore volume

and pore size of the Ni_2P/Al_2O_3 catalyst considerably decreased, compared with those of the Ni/Al_2O_3 catalyst. This might be due to that the volume expansion for the conversion of Ni to Ni_2P further blocked cross section of the initial pores.

2.2. Surface Properties of the Fresh Catalysts

The surface composition, information on the valence states and chemical environment of Ni and P were obtained by the X-ray photoelectron spectroscopy (XPS) technology. Figure 3 shows the XPS spectra in the Ni 2p region for the Ni/Al_2O_3 and Ni_2P/Al_2O_3 catalyst and P 2p region for Ni_2P/Al_2O_3 catalyst. The Ni 2p region (Figure 3a) of the Ni/Al_2O_3 catalyst exhibited a signal centered at 856.4 eV. The peak can be assigned to Ni^{2+} of the unreduced $NiAl_2O_4$ and NiO formed during the passivation [18]. The peak centered at 852.4 eV can be assigned to reduced Ni^0. A broad peak at 861.4 eV was ascribed to strong shake-up process for the Ni $2p_{3/2}$ signal of Ni^{2+}. For the Ni_2P/Al_2O_3 catalyst, Ni 2p core level spectrum contained two signals. The first one is assigned to $Ni^{\delta+}$ in the Ni_2P phase at 853.1 eV, consisted with that reported at 852.7–853.4 eV [19]. The second one of 856.4 eV was associated with Ni^{2+} of the unreduced nickel aluminate and nickel phosphates during a superficial passivation.

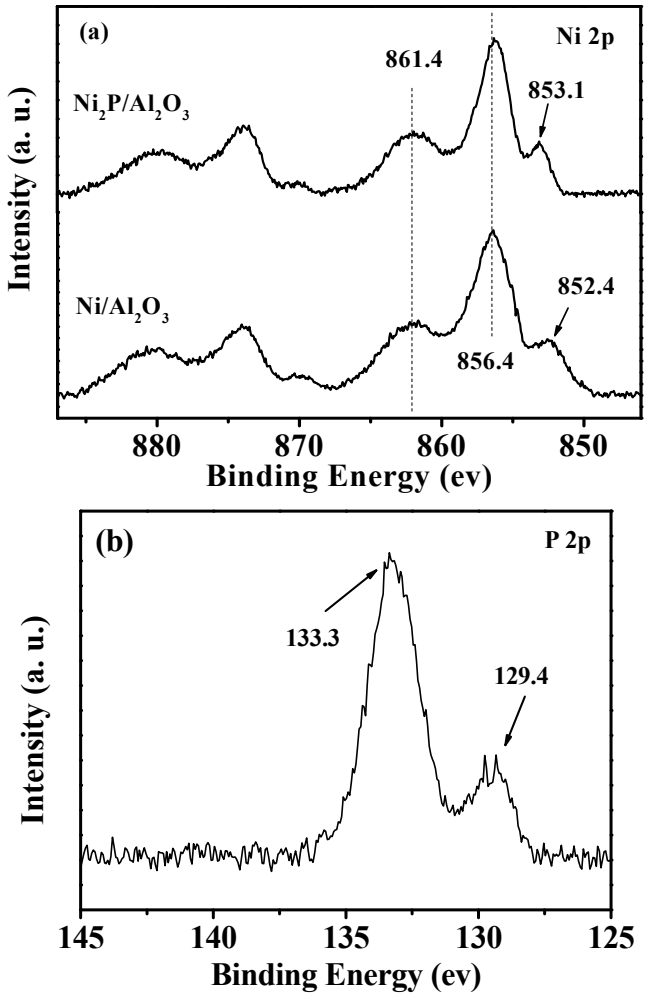

Figure 3. X-ray photoelectron spectroscopy (XPS) spectra of the Ni 2p (**a**) region for the Ni/Al_2O_3 and Ni_2P/Al_2O_3 catalyst and P 2p (**b**) for the Ni_2P/Al_2O_3 catalyst.

The P 2p region for the Ni_2P/Al_2O_3 catalyst is shown in Figure 3b. The peak at 133.3 eV was contributed to P^{5+} of phosphate species formed by the superficial oxidation of Ni_2P during the

passivation. Another peak at 129.4 eV was assigned to reduced $P^{\delta-}$ in Ni_2P, consistent with that reported to be 129.5 eV for $P^{\delta-}$ in metal phosphides [20]. The P ($2p_{3/2}$) binding energy (129.4 eV) was lower than that reported for elemental P (130.2 eV). Simultaneously, the Ni ($2p_{3/2}$) binding energy (853.1 eV) was higher than that reported for Ni^0 (852.4 eV) and lower than that reported for Ni^{2+} (853.5–854.1 eV) [19]. These indicated that the electron density was transferred from Ni to P, and thus the phosphorous had a partial negative charge ($P^{\delta-}$) and the nickel had a partial positive charge ($Ni^{\delta+}$).

Table 2 gives the P/Ni atom ratios from XPS and an inductively coupled plasma atomic emission spectrometer (ICP) analyses. The surface P/Ni atom ratio calculated by XPS analyses was 0.63, almost same as that (0.62) calculated by ICP analyses. This suggested that surplus phosphorous oxides were not formed in the Ni_2P/Al_2O_3 catalyst prepared by triphenylphosphine (PPh_3) phosphidation in liquid phase. Frequently, phosphorous oxides exist largely on the surface of supported Ni_2P catalyst prepared by the temperature programmed reduction method (TPR) and block access to adsorption sites of Ni_2P [21,22]. Thus, the Ni_2P catalyst using the TPR method possessed low density of active site. Remarkably, the P/Ni atom ratio in the Ni_2P/Al_2O_3 catalyst by PPh_3 phosphidation was slightly higher than the Ni_2P stoichiometric ratio (0.5), probably due to the presence of other nickel phosphides with P/Ni stoichiometric ratio >0.5, such as, Ni_5P_4 or NiP_2 [16]. Table 2 also gives the bulk composition of the Ni/Al_2O_3 and Ni_2P/Al_2O_3 catalyst. The loading of Ni in Ni/Al_2O_3 catalyst was 77.9%, similar to the value desired. After phosphidation, the contents of Ni and P in the Ni_2P/Al_2O_3 catalyst were determined to be 60.5% and 19.8%, respectively, also similar to values desired.

Table 2. Chemical composition for the Ni/Al_2O_3 and Ni_2P/Al_2O_3 catalyst.

Catalyst	Ni (wt.%)	P (wt.%)	Al_2O_3 (wt.%)	P/Ni (atom)		Uptake (μmol/g_{cat})	
				ICP	XPS	H_2	CO
Ni/Al_2O_3	77.9	-	22.1	-		979	-
Ni_2P/Al_2O_3	60.5	19.8	19.7	0.62	0.63	-	338

2.3. The Properties of the Used Catalysts

Figure 4 gives the XRD patterns of the Ni/Al_2O_3 and Ni_2P/Al_2O_3 catalyst after the hydrogenation of AP. The results showed that metal Ni phase and Ni_2P phase were the only phase in the used Ni/Al_2O_3 and Ni_2P/Al_2O_3 catalyst, respectively. According to the Scherrer equation, the average crystallite size of metallic Ni and Ni_2P were calculated to be 4.4 and 6.7 nm, respectively. The crystallite size of the Ni and Ni_2P in the used catalysts was almost not changed, compared with that in fresh ones, indicating that metal Ni and Ni_2P had high stability during the hydrogenation reaction.

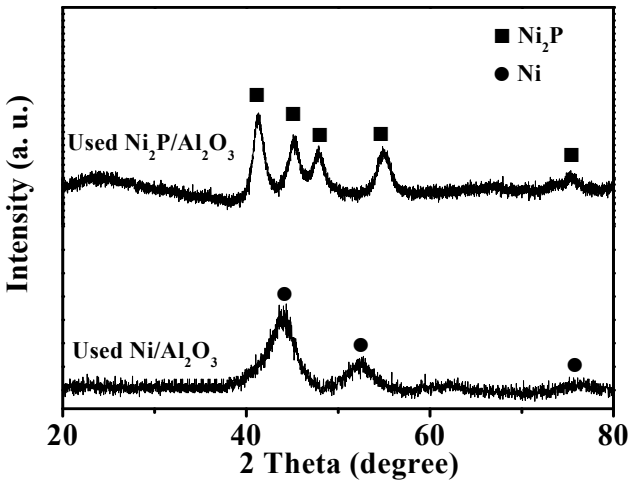

Figure 4. XRD patterns of the used Ni/Al_2O_3 and Ni_2P/Al_2O_3 catalyst.

TEM images of the used Ni/Al_2O_3 and Ni_2P/Al_2O_3 catalyst are shown in Figure 5. The metal Ni and Ni_2P particles were still highly dispersed in the used Ni/Al_2O_3 (Figure 5a) and Ni_2P/Al_2O_3 (Figure 5b) catalyst. The average particle sizes of Ni and Ni_2P were estimated to be 6.0 and 8.0 nm, respectively. Compared with the average particle sizes of Ni (5.8 nm) and Ni_2P (8.2 nm) in the fresh ones, the particle sizes in the used catalyst were almost not changed. These also indicated that metal Ni and Ni_2P had high stability during the hydrogenation reaction.

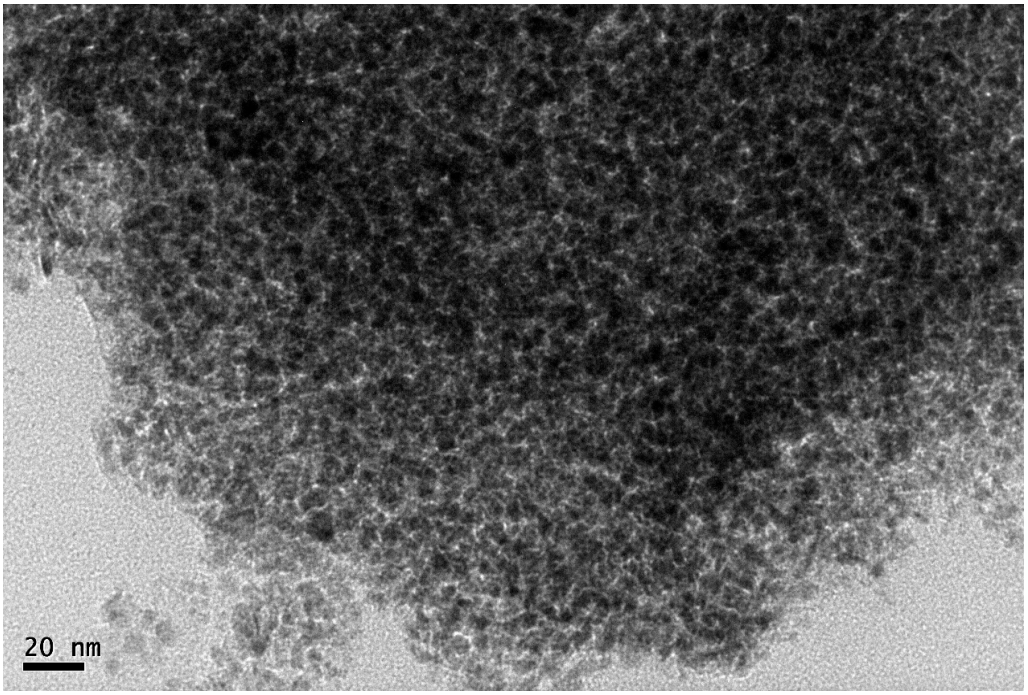

(**a**)

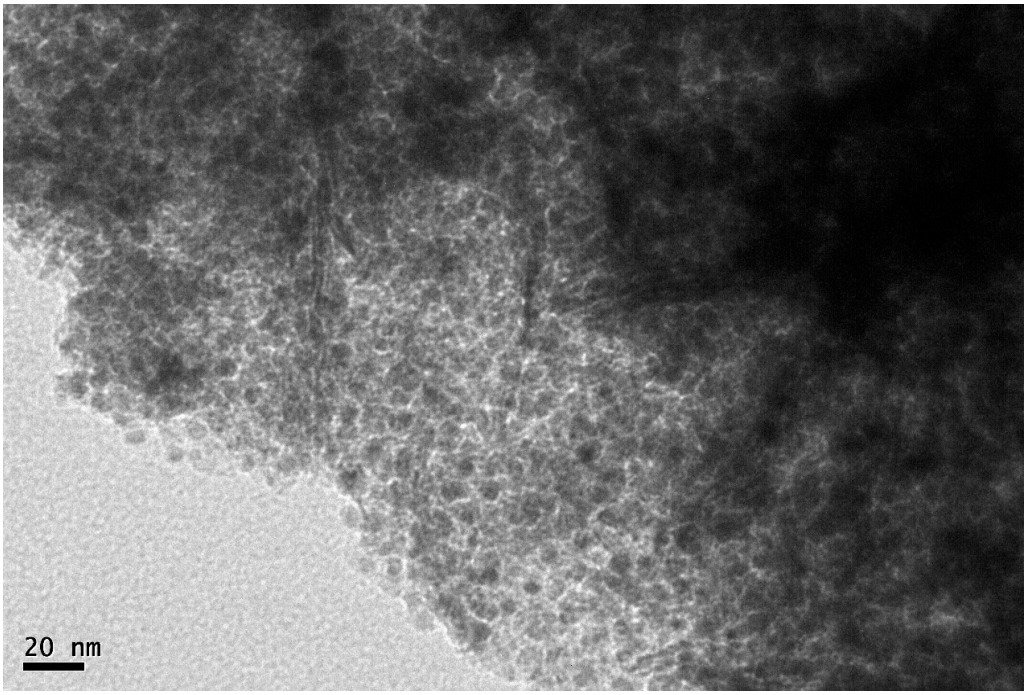

(**b**)

Figure 5. TEM images of the used Ni/Al_2O_3 (**a**) and Ni_2P/Al_2O_3 (**b**) catalyst.

2.4. Catalytic Results

The carbonyl group and aromatic ring of AP can be hydrogenated, and the possible reaction pathways are shown in Figure 6. PHE and CHMK can be obtained through hydrogenation of carbonyl group and aromatic ring, and then further hydrogenated to obtain CHE and EB, respectively.

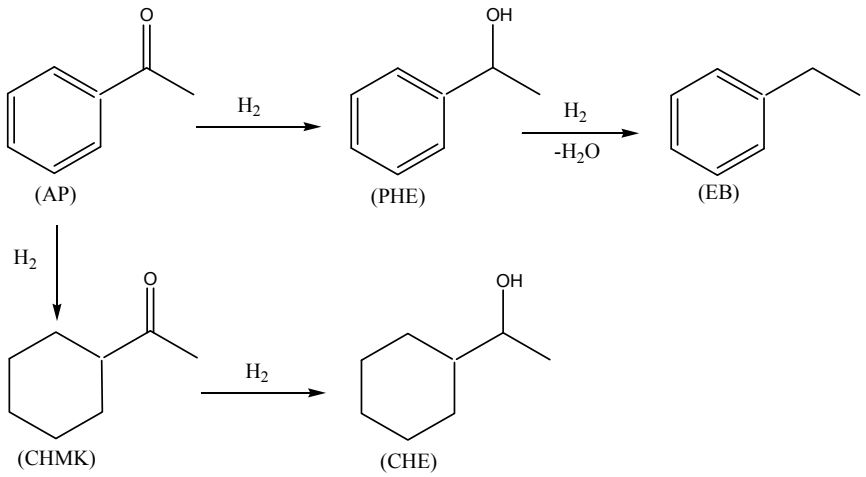

Figure 6. Reaction network of AP hydrogenation on the metal catalysts.

Figure 7 gives the activities and selectivities for hydrogenation of AP at different reaction temperatures on the Ni/Al_2O_3 and Ni_2P/Al_2O_3 catalyst. Figure 7a shows that the conversion of AP increased with the increase of reaction temperature. At 453 K, the conversion of AP reached 100% on both catalysts. At 373 K, the conversions of AP were 77.9% and 41.0% on the Ni/Al_2O_3 and Ni_2P/Al_2O_3 catalyst, respectively, indicating that the apparent activity for hydrogenation of AP on the Ni/Al_2O_3 catalyst was higher than that on the Ni_2P/Al_2O_3 catalyst.

Figure 7b gives the results of selectivity to PHE on the Ni/Al_2O_3 and Ni_2P/Al_2O_3 catalyst. The main products were PHE and CHE on the Ni/Al_2O_3 catalyst. Minor quantities of CHMK and EB were found in the hydrogenation products. The total selectivity to CHMK and EB (not shown) was less than 5%, even though the reaction temperature reached 453 K. At the same temperature, the selectivity to PHE on the Ni/Al_2O_3 catalyst was 12%. However, the hydrogenation products on the Ni_2P/Al_2O_3 catalyst were PHE and CHE, and no CHMK and EB were observed. The selectivity to PHE was 100% at the reaction temperature from 333 K to 373 K. The selectivity of PHE (95.6%) on the Ni_2P/Al_2O_3 was significantly higher than that (12%) on the Ni/Al_2O_3 at 453 K.

To compare the intrinsic activities of Ni/Al_2O_3 and Ni_2P/Al_2O_3 catalyst, the effect of weight hourly space velocity (WHSV) on the hydrogenation of AP at 433 K was performed and shown in Figure 8a. It was found that the conversion of AP on the two catalysts decreased with the increase of WHSV of AP.

The density of active site on surface of Ni and Ni_2P catalysts is generally evaluated by the H_2 and CO uptake, respectively [16,23,24]. The H_2 and CO uptake on the Ni/Al_2O_3 and Ni_2P/Al_2O_3 was determined to be 979 and 338 $\mu mol/g_{cat.}$ (see Table 2), respectively. According to uptakes of chemical adsorption, turnover frequencies (TOF) of AP on the two catalysts can be calculated. The results are shown in Figure 8b. The TOF of AP increased with increase of WHSV and almost reached constant values of about 0.006 and 0.025 s^{-1} at a WHSV of 8 h^{-1} on the Ni/Al_2O_3 and Ni_2P/Al_2O_3, respectively. Apparently, the intrinsic activity of Ni_2P/Al_2O_3 catalyst was much higher than that of Ni/Al_2O_3 catalyst.

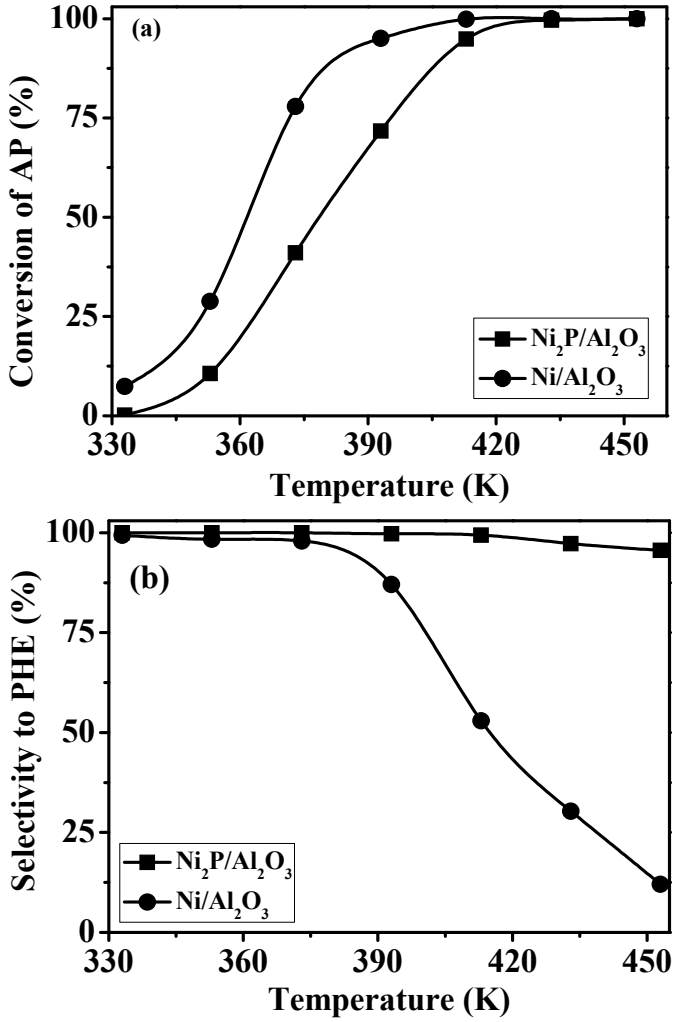

Figure 7. Conversions of AP (**a**) and selectivities to PHE (**b**) over the Ni/Al_2O_3 and Ni_2P/Al_2O_3 catalyst. Reaction conditions: p = 3.0 MPa, H_2/AP = 5, WHSV = 2.

Figure 8c shows the selectivity to PHE against WHSV of AP. The selectivity to PHE on the Ni/Al_2O_3 and Ni_2P/Al_2O_3 catalyst was almost not changed with the increase of WHSV and maintained at about 31% and 98%, respectively. The selectivity to PHE on the Ni_2P/Al_2O_3 was significantly higher than that on the Ni/Al_2O_3, consistent with that reported by Dolly and his co-authors for hydrogenation of AP on the supported nickel phosphides [15]. The results might be caused by the following two reasons. The first one was attributed to the special structure of the active sites on Ni_2P surface. The bond length of Ni-P in Ni_2P and C-C between aromatic ring and carbon atom of the carbonyl group is 0.22 nm and 0.15 nm [25], respectively. This demonstrates that the position of P might be matched with the center of the aromatic ring. From XPS results, it is known that the phosphorous had a partial negative charge ($P^{\delta-}$) in Ni_2P, which repulsed the phenyl group away the surface of catalyst. Simultaneously, the nickel had a partial positive charge ($Ni^{\delta+}$) in Ni_2P, attracting the oxygen atom of carbonyl group to the surface of catalyst. These lead to preferential hydrogenation of carbonyl group. Another reason might be attributed to the effect of supported metal particle size. The selectivity of the hydrogenation reaction is significantly affected by the metal particle size of the catalyst, due to the different adsorption configurations of reactant molecules on the catalysts with different particle size. There are two configurations for the adsorption of AP on the metal catalyst. For the first configuration, the oxygen atoms are linearly absorbed on the surface Ni sites and the carbonyl groups are parallel to the catalyst surface, leading to simultaneous hydrogenation of carbonyl

group and aromatic ring. For the second configuration, the carbonyl groups are adsorbed through the π electrons (bridged adsorption) on the surface Ni sites and the aromatic rings are tilted to the catalyst surface, leading to preferential hydrogenation of carbonyl group [7]. The carbonyl group is mainly absorbed on the catalyst with large metal particle size through the bridged adsorption while on the catalyst with small metal particle size through the linear adsorption [26]. The Ni_2P particle size (8.2 nm) is larger than the Ni particle size (5.8 nm). AP absorption on Ni_2P catalyst had more bridged configuration. Thus, the Ni_2P/Al_2O_3 exhibited higher selectivity to PHE than the Ni/Al_2O_3.

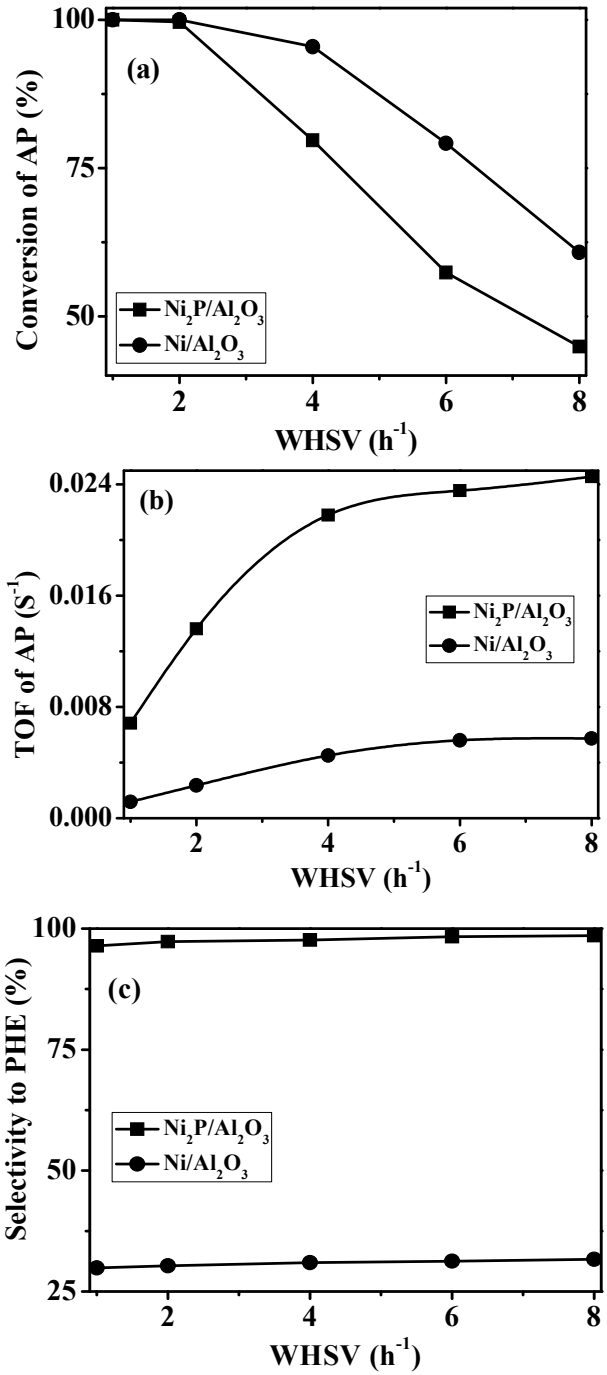

Figure 8. Conversions (**a**), turnover frequencies (TOF) (**b**) of AP and selectivity to PHE (**c**) vs. WHSV of AP over the Ni/Al_2O_3 and Ni_2P/Al_2O_3 catalyst. Reaction conditions: p = 3.0 MPa, H_2/AP = 5, T = 433 K.

3. Materials and Methods

3.1. Catalyst Preparation

The precursor of Ni/Al_2O_3 catalyst with Ni loading of 80 wt.% was prepared by improved co-precipitation method. Briefly, the desired quantities nickel nitrate and aluminum nitrate were dissolved in an aqueous solution of deionized water. The desired amount of sodium carbonate was dissolved in another aqueous solution of deionized water. The above two solutions were simultaneously added into a vessel with 200 mL deionized water at 353 K under continuous stirring. The green precipitates were washed in deionized water six times. The washed precipitates were re-dispersed in 200 mL n-butanol and evaporated at 353 K. Then sample was further dried in electric oven at 393 K to obtain the precursor of Ni/Al_2O_3 catalyst. The precursor was reduced in H_2 (0.1 MPa and 40 mL/min) at 723 K for 2 h and cooled down to a reaction temperature, at which the feeding was fed into the reactor and the hydrogenation of AP began in situ.

The Ni_2P/Al_2O_3 catalyst was prepared by the phosphidation with triphenylphosphine (PPh_3) in liquid phase. The same phosphidation procedure was described previously [16]. Briefly, the Ni/Al_2O_3 catalyst was loaded into a reactor and reduced in H_2 (0.1 MPa and 40 mL/min) at 723 K for 2 h to form Ni/Al_2O_3 catalyst. Then, the temperature was cooled down to 443 K and the Ni/Al_2O_3 was phosphided with PPh_3 (2%) in heptane solution (Liquid hourly space velocity (LHSV) of 2 h^{-1} and H_2/oil of 300 v/v) for 36 h. Afterwards, the sample was treated in H_2 at 673 K for 3 h to form Ni_2P/Al_2O_3 catalyst. The catalyst was then cooled down to a reaction temperature, at which the feeding was fed into the reactor and the hydrogenation of AP began in situ.

3.2. Catalyst Characterization

The Ni/Al_2O_3 and Ni_2P/Al_2O_3 catalyst were prepared separately for characterizations. The preparation was same as those described above. The prepared catalysts were passivated at room temperature under 0.5 vol.% O_2 in N_2 for 12 h and then characterized by different techniques.

TEM was obtained on a JEM-2100 (JEOL, Tokyo, Japan) high-resolution microscope operating at 200 kV. The samples were dispersed in 5% ethanol solution and dropped onto a copper grid coated with a carbon film.

XRD patterns were recorded on a D8 Advance powder diffractometer (Bruker Biosciences Corporation, Billerica, MA, USA) using a Cu Kα source (λ = 0.1541 nm) at 40 KV and 40 mA. The 2θ scans covered the range of 20 to 80° with a step of 0.02°.

The specific surface areas (S_{BET}), pore volume and pore size were measured at 77.3 K using a Micromeritics Gemini V 2380 autosorption analyzer (Micromeritics Corporation, Norcross, GA, USA).

XPS measurements were carried out by a Thermo ESCALAB 250 (Thermo Fisher Scientific, Waltham, MA, USA) with Al Kα (1486.6 eV) line at 150 W.

The chemical compositions of the catalysts were obtained using an inductively coupled plasma atomic emission spectrometer (ICP-AES, ICPS-7510, Shimadzu Corporation, Tokyo, Japan).

H_2 and CO chemisorption isotherms at 308 K were performed to measure H_2 and CO uptake of Ni/Al_2O_3 and Ni_2P/Al_2O_3, respectively. The precursor of Ni/Al_2O_3 catalyst was reduced in H_2 at 723 K for 2 h while the passivated Ni_2P/Al_2O_3 catalyst was re-reduced in H_2 at 673 K for 3 h and then evacuated at the corresponding reduction temperature for 1 h. After cooling to 308 K, the chemisorption of H_2 or CO was performed. The uptakes of H_2 and CO were estimated by extrapolating the linear portion of the isotherm to $p = 0$.

3.3. Catalytic Tests

The hydrogenation of AP was carried out at 3.0 MPa pressure in a continuous flow fixed-bed microreactor (inner diameter 10 mm). The catalyst sample of 1.0 g (40–60 mesh) was mixed with quartz sand. The feeding consisted of a solution of 33.3 wt.% AP in ethanol and the H_2/AP was 5 (molar ratio). The products were analyzed by a gas chromatograph equipped with a flame ionization

detector (FID) and a HP-FFAP capillary column. The TOF was calculated by dividing the number of molecules converted per second by the number of active nickel atoms on the surface measured by H_2 (for Ni/Al_2O_3) or CO (for Ni_2P/Al_2O_3) adsorption.

4. Conclusions

A highly dispersed and loaded Ni/Al_2O_3 catalyst was prepared by the co-precipitation and subsequently phosphided by PPh_3 in liquid phase to form Ni_2P/Al_2O_3 catalyst, which possessed high dispersion and loading of Ni_2P. XPS results showed that the phosphorous had a partial negative charge ($P^{\delta-}$) and the nickel had a partial positive charge ($Ni^{\delta+}$) on the surface of Ni_2P/Al_2O_3 catalyst.

The hydrogenation of AP was performed on the Ni/Al_2O_3 and Ni_2P/Al_2O_3 catalyst. The results showed that the Ni/Al_2O_3 catalyst had higher apparent activity than the Ni_2P/Al_2O_3 catalyst. However, the Ni_2P/Al_2O_3 catalyst possessed higher intrinsic activity than the Ni/Al_2O_3 catalyst. In particular, the Ni_2P/Al_2O_3 catalyst exhibited higher selectivity to PHE than the Ni/Al_2O_3 catalyst. This might be caused by the following two reasons. First, $Ni^{\delta+}$ in Ni_2P attracted the oxygen atom of carbonyl group to the surface of catalyst while $P^{\delta-}$ in Ni_2P repulsed the phenyl group away the surface of catalyst, leading to preferential hydrogenation of carbonyl group in AP. Second, the effect of particle size of Ni_2P catalyst might be another reason for high selectivity to PHE.

Author Contributions: J.W., Y.W., G.C. designed and performed the experiments; Z.H. analyzed the experiment data; J.W. wrote this paper.

Funding: This research received no external funding.

Acknowledgments: The work was financially supported by the Natural Science Foundation of Educational Committee of Anhui Province (Nos. KJ2017A382, KJ2016B008, KJ2017B003 and KJ2017A389), the Program for Outstanding Young Talents in Higher Education Institutions of Anhui Province (No. gxyqZD2018048) and the Open Fund of Advanced Functional Composite Materials of Anhui Province (XTZX103732016003).

Conflicts of Interest: The authors declare no conflicts of interest.

References

1. Finlayson, B.A.; Biegler, L.T.; Grossmann, I.E. *Ullmann's Encyclopedia of Industrial Chemistry*; Wiley-VCH: Weinheim, Germany, 2006.
2. Casagrande, M.; Storaro, L.; Talon, A.; Lenarda, M.; Frattini, R.; Rodríguez-Castellón, E.; Maireles-Torres, P. Liquid phase acetophenone hydrogenation on Ru/Cr/B catalysts supported on silica. *J. Mol. Catal. A* **2002**, *188*, 133–139. [CrossRef]
3. Červený, L.; Bělohlav, Z.; Hamed, M.N.H. Catalytic hydrogenation of aromatic aldehydes and ketones over ruthenium catalysts. *Res. Chem. Intermed.* **1996**, *22*, 15–22. [CrossRef]
4. Aramendia, M.A.; Borau, V.; Gomez, J.F.; Herrera, A.; Jimenez, C.; Marinas, J.M. Reduction of acetophenones over $Pd/AlPO_4$ catalysts. Linear free energy relationship (LFER). *J. Catal.* **1993**, *140*, 335–343. [CrossRef]
5. Drelinkiewicza, A.; Waksmundzka, A.; Makowski, W.; Sobczak, J.W.; Król, A.; Zieba, A. Acetophenone hydrogenation on polymer-palladium catalysts: The effect of polymer matrix. *Catal. Lett.* **2004**, *94*, 143–156. [CrossRef]
6. Santori, G.F.; Moglioni, A.G.; Vetere, V.; Iglesias, G.Y.M.; Casella, M.L.; Ferretti, O.A. Hydrogenation of aromatic ketones with Pt- and Sn-modified Pt catalysts. *Appl. Catal. A Gen.* **2004**, *269*, 215–223. [CrossRef]
7. Chen, C.-S.; Chen, H.-W.; Cheng, W.-H. Study of selective hydrogenation of acetophenone on Pt/SiO_2. *Appl. Catal. A Gen.* **2003**, *248*, 117–128. [CrossRef]
8. Zaccheria, F.; Ravasio, N.; Psaro, R.; Fusi, A. Heterogeneous selective catalytic hydrogenation of aryl ketones to alcohols without additives. *Tetrahedron Lett.* **2005**, *46*, 3695–3697. [CrossRef]
9. Bertero, N.M.; Apesteguía, C.R.; Marchi, A.J. Catalytic and kinetic study of the liquid-phase hydrogenation of acetophenone over Cu/SiO_2 catalyst. *Appl. Catal. A Gen.* **2008**, *349*, 100–109. [CrossRef]
10. Bertero, N.M.; Apesteguía, C.R.; Marchi, A.J. One-pot synthesis of olefins from aromatic ketones via tandem consecutive hydrogenation–dehydration reactions. *Catal. Today* **2011**, *172*, 171–176. [CrossRef]

11. Trasarti, A.F.; Bertero, N.M.; Apesteguía, C.R.; Marchi, A.J. Liquid-phase hydrogenation of acetophenone over silica-supported Ni, Co and Cu catalysts: Influence of metal and solvent. *Appl. Catal. A Gen.* **2014**, *475*, 282–291. [CrossRef]
12. Rajashekharam, M.V.; Bergault, I.; Fouilloux, P.; Schweich, D.; Delmas, H.; Chaudhari, R.V. Hydrogenation of acetophenone using a 10% Ni supported on zeolite Y catalyst: Kinetics and reaction mechanism. *Catal. Today* **1999**, *48*, 83–92. [CrossRef]
13. Malyala, R.V.; Rode, C.V.; Arai, M.; Hegde, S.G.; Chaudhari, R.V. Activity, selectivity and stability of Ni and bimetallic Ni-Pt supported on zeolite Y catalysts for hydrogenation of acetophenone and its substituted derivatives. *Appl. Catal A Gen.* **2000**, *193*, 71–86. [CrossRef]
14. Bertero, N.M.; Trasarti, A.F.; Apesteguía, C.R.; Marchi, A.J. Solvent effect in the liquid-phase hydrogenation of acetophenone over Ni/SiO_2: A comprehensive study of the phenomenon. *Appl. Catal. A Gen.* **2011**, *394*, 228–238. [CrossRef]
15. Dolly, C.C.; Analía, L.S.; Gina, P.; José Fernando, B.; Sergio Gustavo, M.; Virginia, V. Preparation and characterization of a supported system of $Ni_2P/Ni_{12}P_5$ nanoparticles and their use as the active phase in chemoselective hydrogenation of acetophenone. *Nanotechnology* **2018**, *29*, 215702.
16. Wang, J.; Chen, H.; Fu, Y.; Shen, J. Highly active Ni_2P/SiO_2 catalysts phosphorized by triphenylphosphine in liquid phase for the hydrotreating reactions. *Appl. Catal. B Environ.* **2014**, *160–161*, 344–355. [CrossRef]
17. Wang, J.; Fu, Y.; Chen, H.; Shen, J. Effect of supports on the supported Ni_2P catalysts prepared by the phosphidation using triphenylphosphine in liquid phase. *Chem. Eng. J.* **2015**, *275*, 89–101. [CrossRef]
18. Huang, Y.J.; Schwarz, J.A.; Diehl, J.R.; Baltrus, J.P. Effect of catalyst preparation on catalytic activity: V. Chemical structures on nickel/alumina catalysts. *Appl. Catal.* **1988**, *36*, 163–175. [CrossRef]
19. Briggs, D.; Seah, M.P. *Practical Surface Analysis: By Auger and X-ray Photoelectron Spectroscopy*; Wiley: Hoboken, NJ, USA, 1983.
20. Cecilia, J.A.; Infantes-Molina, A.; Rodriguez-Castellon, E.; Jimenez-Lopez, A. A novel method for preparing an active nickel phosphide catalyst for HDS of dibenzothiophene. *J. Catal.* **2009**, *263*, 4–15. [CrossRef]
21. Sawhill, S.J.; Layman, K.A.; Van Wyk, D.R.; Engelhard, M.H.; Wang, C.; Bussell, M.E. Thiophene hydrodesulfurization over nickel phosphide catalysts: Effect of the precursor composition and support. *J. Catal.* **2005**, *231*, 300–313. [CrossRef]
22. Prins, R.; Bussell, M.E. Metal phosphides: Preparation, characterization and catalytic reactivity. *Catal. Lett.* **2012**, *142*, 1413–1436. [CrossRef]
23. Xue, M.; Hu, S.; Chen, H.; Fu, Y.; Shen, J. Preparation of highly loaded and dispersed Ni/SiO_2 catalysts. *Catal. Commun.* **2011**, *12*, 332–336. [CrossRef]
24. Oyama, S.T.; Lee, Y.-K. The active site of nickel phosphide catalysts for the hydrodesulfurization of 4,6-DMDBT. *J. Catal.* **2008**, *258*, 393–400. [CrossRef]
25. Jun, R.E.N.; Wang, J.G.; Li, J.F.; Li, Y.W. Density functional theory study on crystal nickel phosphides. *J. Fuel Chem. Technol.* **2007**, *35*, 458–464.
26. Yates, J.T., Jr.; Garland, C.W. Infrared studies of carbon monoxide chemisorbed on nickel and on mercury-poisoned nickel surfaces. *J. Phys. Chem.* **1961**, *65*, 617–624. [CrossRef]